Milli-Kelvin NQR: A Study of the Praseodymium Trihalides *

Robin L. Armstrong
Department of Physics, University of New Brunswick, Fredericton, N.B., Canada

Sunyu Su
Department of Physics, University of Toronto, Toronto, Ontario, Canada

Z. Naturforsch. **47a**, 221–226 (1992); received August 8, 1991

Milli-Kelvin NQR experiments are often essential for the study of pseudo one-dimensional materials. A brief overview of the special technical consideration for carrying out NQR measurements in a dilution refrigerator is given. Recent halide quadrupole resonance experiments on the pseudo one-dimensional XY crystals $PrCl_3$ and $PrBr_3$ are reviewed including the measurement and interpretation of frequencies, and spin-lattice relaxation times.

I. Introduction

The physics of one-dimension is particularly appealing because of its relative theoretical simplicity. Unlike the physics of three-dimensions it is often possible to carry out exact calculations, or at least to know the consequences of the approximations that are being made. The difficulty is in finding crystals which provide experimental realizations of the one-dimensional model systems. Often when such systems are identified, the temperature range over which the one-dimensional behaviour manifests itself is very inconvenient, occurring in the milli-Kelvin regime. The praseodymium trihalides are a case in point. They are among the best physical realizations of the XY chain, but the temperature range of interest extends from the order of 100 mK to 4 K.

II. NQR Probe

A dilution refrigerator [1] is an ideal instrument for obtaining temperatures in the milli-Kelvin range. The challenge in using a dilution refrigerator for an NQR experiment is to obtain a successful balance between the low heat capacity of the dilution refrigerator and the unavoidable heating which accompanies the rf excitation of the resonance. A rf co-axial cable is essential for the experiment, but the overall Ohmic heat generated in the coil and the heat leak from the co-axial cable, factors which are negligible in a conventional NQR experiment, are now significant and must be given special consideration.

Figure 1 shows the NQR probe. The sample container was a 0.5 in. diameter pyrex tube, 1.5 in. in length. A copper flange was attached to the top and an indium seal was used to seal the container to a copper piece which was screwed to the bottom of the finger from the mixing chamber. About 40 copper wires were soldered to the flange and immersed in the liquid helium in the sample tube during the experiments in order to enhance the thermal conduction. Liquid helium was supplied to the sample tube from the 1 K pot via a thin stainless steel tube.

The rf coil was wound on a cylindrical delrin coil former with a space between the former and the sample tube. During an experiment this space was evacuated to minimize the transmission of heat into the sample. The tuning capacitors were attached to the top portion of the coil former. The coil was pre-tuned as close to the resonance frequency as possible so that maximum rf power transmission could be achieved. This was particularly important for the bromine resonances studied, because in this case the rf wave length is of the same order of magnitude as the dimensions of the probe including the co-axial line.

The choice of co-axial cable is crucial as it represents a large potential heat leak. We chose a commercially available, 50 ohm, semi-rigid micro-cable (outer diameter 0.085 in.), 40 in. in length, with stainless steel inner and outer conductors. By anchoring the outer conductor to the 4 K pot, the amount of heat leaked to the sample area was reduced to well less than

* Presented at the XIth International Symposium on Nuclear Quadrupole Resonance Spectroscopy, London, United Kingdom, July 15–19, 1991.

Reprint requests to Dr. R. L. Armstrong, Department of Physics, University of New Brunswick, Fredericton, N.B., Canada.

0932-0784 / 92 / 0100-0221 $ 01.30/0. – Please order a reprint rather than making your own copy.

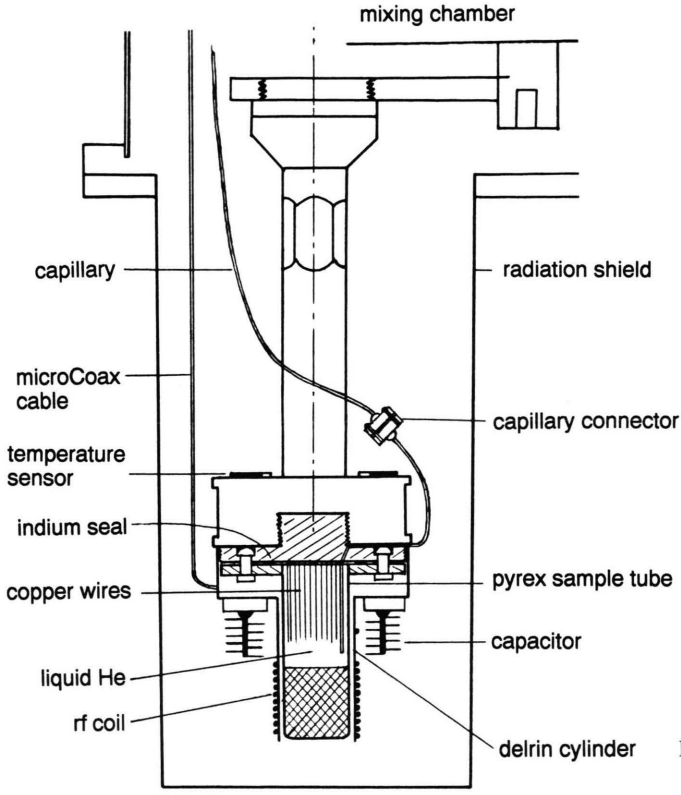

Fig. 1. Milli-Kelvin NQR probe.

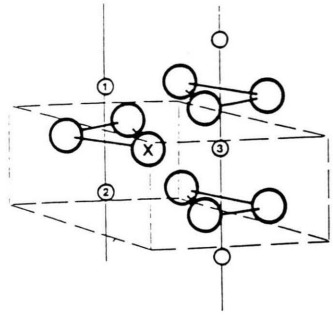

Fig. 2. Crystal structure of PrX_3. The large circles denote X ions; the small circles, Pr ions. Pr ions labelled 1, 2 and 3 are nearest neighbours to the labelled X ion. The dashed lines indicate a unit cell.

200 μW, which was within the capacity of the dilution refrigerator that was available.

Temperatures were measured using two germanium temperature sensors calibrated by the manufacturers. We were able to obtain sample temperatures down to about 125 mK; in principle, the dilution refrigerator should have been able to generate temperatures to 50 mK, but it was in need of maintenance.

III. Samples

Using the dilution refrigerator, measurements of the halide NQR resonances for $PrCl_3$ and $PrBr_3$ were carried out. Frequencies and spin-lattice relaxation times were measured.

Both samples crystallize in an hexagonal structure as indicated schematically in Figure 2. The small circles denote Pr ions; the large circles X ions. Pr ions 1, 2 and 3 are nearest neighbours to the designated X ion. The dashed lines indicate a unit cell. The Pr ions form linear chains along the hexagonal crystal axes.

The electronic ground state of a free Pr ion in ninefold degenerate. The degeneracy is partially lifted by the presence of the crystal electric field at a Pr-ion site. The energy separation of the first excited state from the ground state doublet is 17 K for $PrBr_3$ and 46 K for $PrCl_3$. Below 4 K the Pr ions are for practical purposes all in the ground state so that an effective spin 1/2 representation is appropriate to describe the Pr–Pr interactions. The pseudo-spin has an associated magnetic moment parallel to the hexagonal axis; it is rather small and gives rise to a small $S_z^i S_z^j$ magnetic dipole-dipole interaction. In addition, the strong coupling between the ground state doublet and the transverse distortions gives rise to a large XY interaction. The distortion transforms as (x, y) and therefore carries an electric dipole moment. In an effective spin 1/2 representation, this XY interaction can be expressed in terms of electric dipole pseudo-spin operators as $[S_x^i S_x^j + S_y^i S_y^j]$. The dominant term in the Hamiltonian describing the Pr–Pr interaction is the electric dipole interaction between the i-th and $(i+1)$th spins along the hexagonal axes. Therefore, to a good approximation, the Hamiltonian describing

the Pr–Pr interaction between nearest neighbour spins along the chains has the form

$$\mathcal{H}_{i,i+1} = J(S_x^i S_x^{i+1} + S_y^i S_y^{i+1}).$$

That is, the praseodymium trihalides provide a good approximation to the ideal XY chain.

IV. NQR Frequencies [2, 3]

Figure 3 a shows the temperature dependence of the ^{35}Cl NQR frequency. The single frequency at high temperatures symmetrically splits into two components of equal intensity at 0.428 K with the spectral centre of mass being conserved through the phase transition. Figure 3 b shows the temperature dependence of the ^{81}Br NQR frequency. The behaviour is similar except that the phase transition occurs at 0.130 K, significantly lower than for $PrCl_3$. Based on a group theoretical analysis [4], it has been concluded that the phase transition is a co-operative Jahn-Teller transition to a 3-D antiferroelectric ordered state which was predicted to be a Peierls dimerization.

For a dimerized structure, the separation of neighbouring Pr ions along the chain alternates, long, short, long, short etc. As a result the field gradient parameter V_{zz} and asymmetry parameter η are changed and hence so is the NQR frequency. A point charge model was used to calculate the irreducible components of the electric field gradient tensor both above and below the phase transition. Contribution from 900 unit cells were included. Assuming that the anti-shielding factor required to relate the electric field gradient as calculated by the point charge model to the actual field gradient is the same above and below the phase transition, the results should provide a reliable measure of the dimerization. We are therefore able to calculate a dimerization parameter

$$D = |r_0(\mathrm{Pr}) - r(\mathrm{Pr})|,$$

where r_0(Pr) is the separation of nearest neighbour Pr ions in the high temperature phase and r(Pr) the separation in the dimerized phase. The deduced measure of dimerization is $D/c = 0.007$ for both compounds.

V. Spin-Lattice Relaxation [5, 6]

Halide spin-lattice relaxation times were measured in the one-dimensional temperature regime for the

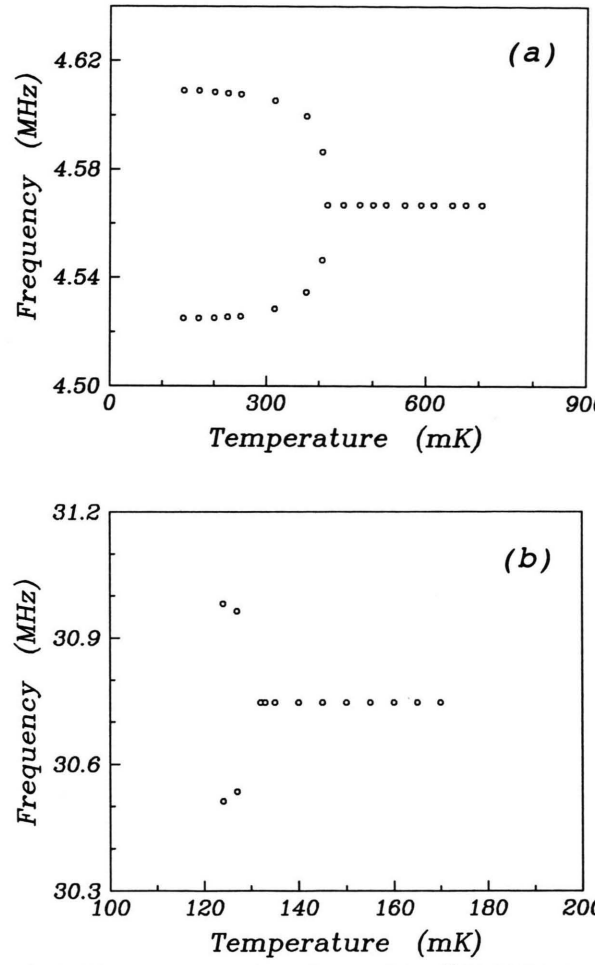

Fig. 3. (a) Temperature dependence of the ^{35}Cl NQR frequency in $PrCl_3$; (b) temperature dependence of the ^{81}Br NQR frequency in $PrBr_3$.

^{35}Cl isotope in $PrCl_3$ and the ^{79}Br and ^{81}Br isotopes in $PrBr_3$. To minimize rf heating of the sample a $\pi/2-\pi/2$ pulse sequence was used with a repetition rate ot 30 sec. The pulse lengths were 17 μsec for the chlorine resonance and 5.5 μsec for the bromine resonances. No signal averaging was required. Typical magnetization recovery curves are shown in Fig. 4; a chlorine recovery curve in Fig. 4a and a bromine recovery curve in Figure 4b. In each case the recovery is exponential as expected for a spin 3/2 system. Note that the recovery of the bromine magnetization is an order of magnitude faster than the recovery of the chlorine magnetization. This result reflects the much larger magnetic hyperfine coupling constant for

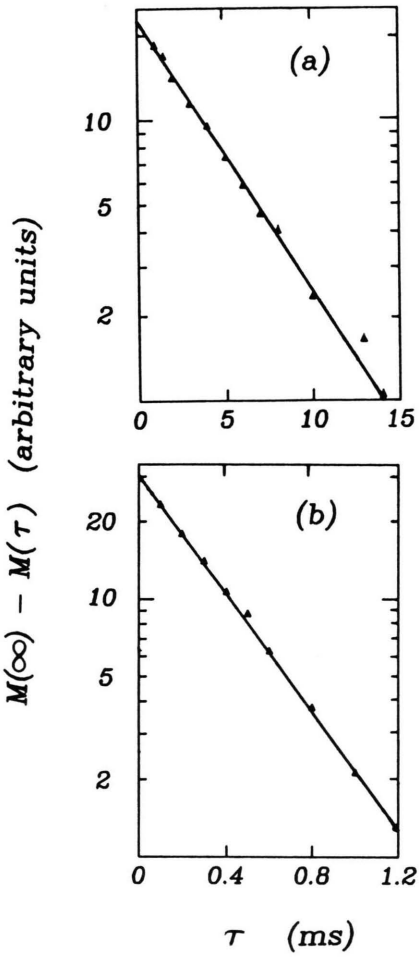

Fig. 4. Magnetization recovery curves: (a) for the ^{35}Cl resonance in $PrCl_3$ at 4.2 K; (b) for the ^{81}Br resonance in $PrBr_3$ at 2.4 K.

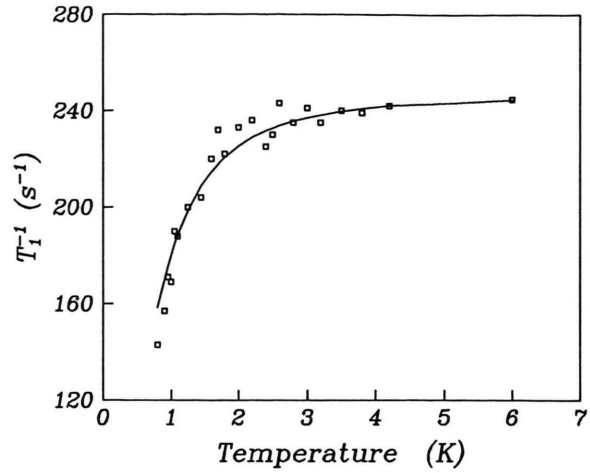

Fig. 5. Temperature dependence of T_1^{-1} for ^{35}Cl in $PrCl_3$. The squares are experimental data. The solid line is the theoretical prediction for $J/k_B = 2.2$ K.

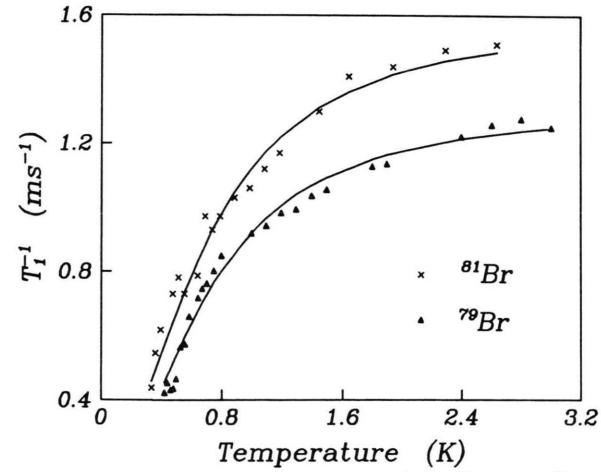

Fig. 6. Temperature dependences of T_1^{-1} for ^{79}Br and ^{81}Br nuclei in $PrBr_3$. The triangles and crosses are experimental data. The solid lines are the theoretical predictions for $J/k_B = 2.35$ K.

bromine nuclei as compared to chlorine nuclei. The temperature dependence of T_1^{-1} for the ^{35}Cl resonance is shown in Fig. 5 and that for the ^{79}Br and ^{81}Br resonances in Figure 6. Note in this latter case that the ^{81}Br data lie above the ^{79}Br data. This observation provides a dramatic illustration that the spin-lattice relaxation process is dominated by the magnetic dipole interaction and not by the electric quadrupolar interaction. If the latter were true, the ^{81}Br data would lie below the ^{79}Br data. This follows from the fact that the ratio of the squares of the magnetic moments is $[\mu(^{79}Br)/\mu(^{81}Br)]^2 = 0.861$ while the ratio of the squares of the electric quadrupole moments is $[Q(^{79}Br)/Q(^{81}Br)]^2 = 1.4$.

A general expression for the spin-lattice relaxation rate due to a fluctuating magnetic field $H_q(t)$ at the site of a resonant nucleus is given by [7]

$$T_1^{-1} = \gamma_n^2 [k_{xx}(\omega_0) + k_{yy}(\omega_0)],$$

where γ_n is the nuclear gyromagnetic ratio, ω_0 is the resonance frequency and k_{qq}, is the spectral density of the fluctuating magnetic field as given by

$$k_{qq'}(\omega) = \tfrac{1}{2} \int_{-\infty}^{\infty} \langle H_q(t)\, H_{q'}(0) \rangle\, e^{i\omega t}\, dt,$$

where the angular bracket denotes an ensemble average.

It is a reasonable approximation to assume that the fluctuating magnetic field at an X-nuclear site arises solely from the electronic magnetic moments of the three nearest neighbour Pr ions (see Fig. 2); these magnetic moments are parallel to the hexagonal c-axis. The magnetic fields generated at the X-site by the Pr ions labelled 1 and 2 have components parallel and perpendicular to the hexagonal axis; the magnetic field generated by the Pr ion labelled 3 has only a parallel component. It is only the perpendicular components that contribute to spin-lattice relaxation.

The coupling between the resonant X nuclear magnetic moment and the fluctuating magnetic field generated by the Pr ions is assumed to be a magnetic hyperfine interaction of the form $AS_z^m I_z$, where S_z^m is the electronic spin of the Pr ion labelled m, I_z is the z-component of the nuclear angular momentum and A is the hyperfine interaction constant. It follows that T_1^{-1} is given by

$$T_1^{-1} = A^2 \int_{-\infty}^{\infty} [\Phi_{zz}^{11}(t) - \Phi_{zz}^{12}(t)]\, e^{i\omega t}\, dt,$$

where $\Phi_{zz}^{11}(t) = \langle S_z^1(t)\, S_z^1(0)\rangle$ and $\Phi_{zz}^{12}(t) = \langle S_z^1(t)\, S_z^2(0)\rangle$ are the longitudinal spin auto-correlation and pair-correlation functions, respectively. Denoting the Fourier transform of the two correlation functions as $\Phi_{zz}^{11}(\omega)$ and $\Phi_{zz}^{12}(\omega)$, we can write the expression for T_1^{-1} in the compact form

$$T_1^{-1} = A^2 [\Phi_{zz}^{11}(\omega) - \Phi_{zz}^{12}(\omega)].$$

In the 1-D regime, the time dependent longitudinal spin correlation function $\Phi_{zz}^{mn}(t)$ for a spin 1/2 XY model system has been given by Katsura and coworkers [8]. Using this result, the Fourier transforms of the longitudinal spin auto-correlation and pair-correlation functions can be obtained, and the spin-lattice relaxation rate expressed as

$$T_1^{-1} = \left(\frac{A^2\hbar}{\pi J}\right) \int_0^{1-\tilde{\omega}/2} dx\, \frac{[1+\tanh(\beta\tilde{\omega}/4)]^2\,[1+\operatorname{sech}^2\{(\beta\tilde{\omega}/4)\sinh^2(\beta x/2)\}]^{-1}}{[(1+\tilde{\omega}/2)^2 - x^2]^{1/2}\,[(1-\tilde{\omega}/2)^2 - x^2]^{1/2}} \left(x^2 - \frac{\tilde{\omega}^2}{4}\right),$$

where $\tilde{\omega} = \hbar\omega/J$ with J the exchange parameter.

A general analytic expression for T_1^{-1} is unobtainable, and neither the high temperature nor low temperature approximations, for which analytic expressions can be derived, is appropriate in the present case since the temperature range of interest is comparable to J/k_B. Theoretical predictions of the temperature dependence of T_1^{-1} were made by numerical integration of the full expression for a series of temperatures. To do this a value of J was chosen and the parameter A obtained by fitting the theory to the limiting high temperature value of T_1^{-1}. For this value of A the temperature dependence of T_1^{-1} was deduced. The entire process was repeated for a series of values of J and the resultant family of curves was compared to the experimental data to obtain a best fit.

The final theoretical curves* are shown superimposed on the data. Figure 5 shows the situation for the ^{35}Cl data. The parameters describing the solid curve are $A = (1.44 \pm 0.02) \times 10^7\ \text{sec}^{-1}$ and $J/k_B = (2.20 \pm 0.20)$ K. The fitted value of A compares favourably with an estimated, albeit simplistic, calculated value, and the value of J/k_B is in agreement with the most recent published value from a Raman scattering experiment [9]. It is instructive to note that the auto-correlation and pair-correlation function contributes are comparable. Figure 6 shows the situation for the ^{79}Br and ^{81}Br data. The parameter $J/k_B = (2.35 \pm 0.20)$ K in each case. Since J/k_B is a measure of the Pr–Pr interaction strength between nearest neighbours along a chain and has nothing to do with the X nucleus, we indeed expect J/k_B to be isotope independent. The parameter A is, however, isotope sensitive. In particular, $A(^{79}\text{Br}) = (3.54 \pm 0.02) \times 10^7\ \text{sec}^{-1}$ and $A(^{81}\text{Br}) = (3.92 \pm 0.02) \times 10^7\ \text{sec}^{-1}$. The ratio of A^2 values is in agreement with the ratio of the squares of the nuclear magnetic moments as indeed it should be:

$$[A(^{81}\text{Br})/A(^{79}\text{Br})]^2 = 1.22 \pm 0.01;$$

$$[\mu(^{81}\text{Br})/\mu(^{79}\text{Br})]^2 = 1.16.$$

This experiment has provided a direct and rigorous test of the dynamical properties of the 1D XY model.

VI. Summary

This manuscript has described an NQR investigation of the halide resonances in two praseodymium

* Some of the parameters in [6] are incorrect.

trihalides in the milli-Kelvin temperature range. The measurements of the temperature dependence of the resonance frequencies have revealed a phase transition to a dimerized state and provided a quantitative estimate of the dimerization parameter. The measurements of the temperature dependence of the spin-lattice relaxation rates have provided a rigorous test of the dynamical predictions of the theory of a 1-D XY system.

[1] D. S. Betts, An Introduction to Millikelvin Technology, Cambridge University Press, 1989.
[2] J. H. Colwell, B. W. Mangum, and D. B. Utton, Phys. Rev. **181,** 842 (1969).
[3] S. Su, R. L. Armstrong, and W. Wei, to be published (1992).
[4] R. M. Morra, R. L. Armstrong, and D. R. Taylor, Phys. Rev. Lett. **51,** 809 (1983).
[5] B. W. Mangum and D. D. Thornton, Phys. Rev. Lett. **22,** 1105 (1969).
[6] S. Su, R. L. Armstrong, W. Wei, and R. Donaberger, Phys. Rev. **B43,** 7565 (1991).
[7] C. P. Slichter, Principles of Magnetic Resonance, Springer-Verlag, New York, 1990.
[8] S. Katsura, T. Horiguchi, and M. Suzuki, Physica (Utrecht) **46,** 67 (1970).
[9] E. Goovaerts, D. De Readt, and D. Schoemaker, Phys. Rev. Lett. **52,** 1649 (1984).